Single-Molecule Nanocatalysis Hot Paper

International Edition: DOI: 10.1002/anie.201511071
German Edition: DOI: 10.1002/ange.201511071

Single-Molecule Nanocatalysis Shows In Situ Deactivation of Pt/C Electrocatalysts during the Hydrogen-Oxidation Reaction

*Yuwei Zhang, Tao Chen, Shaun Alia, Bryan S. Pivovar, and Weilin Xu**

Abstract: *By coupling a Pt-catalyzed fluorogenic reaction with the Pt-electrocatalyzed hydrogen-oxidation reaction (HOR), we combine single-molecule fluorescence microscopy with traditional electrochemical methods to study the real-time deactivation kinetics of a Pt/C electrocatalyst at single-particle level during electrocatalytic hydrogen-oxidation reaction. The decay of the catalytic performance of Pt/C could be mainly attributed to the electrocatalysis-induced etching or dissolution of Pt nanoparticles. Spontaneous regeneration of activity and incubation period of the Pt electrocatalyst were also observed at single-particle level. All these new insights are practically useful for the understanding and rational design of highly efficient electrocatalysts for application in fuel cells.*

Understanding and controlling the long-term operation stability of nanocatalysts is vitally important in a variety of applications such as nanoscale electronics,[1] sensing,[2] and catalysis.[3] For a practical application of any catalytic materials in fuel cells,[4] the electrode materials (electrocatalysts) must survive hundreds of thousands of load cycles and tens of thousands of start-up and shut-down events over the 5000-hour lifetime.[5] In fuel cells, carbon-supported platinum (Pt/C) has been extensively used as anode electrocatalyst for the hydrogen-oxidation reaction (HOR) or cathode for the oxygen-reduction reaction (ORR).[6] However, because of the complexity of the porous electrode used in traditional ensemble experiments, the variation or deactivation process of Pt/C catalysts under working condition is still not clearly understood.[7] For instance, one of the most significant problems hindering the large-scale application of proton exchange membrane fuel cells is the performance decay of fuel cells induced by the gradual loss of catalytic activity of Pt/C.[8] Developing an electrocatalyst with long-term operation stability requires a deep understanding to the deactivation mechanism during the long-term operation process at microscale level (e.g. at single-molecule and single-nanoparticle levels). In recent years, single-molecule fluorescence microscopy (SMFM) has emerged as a powerful tool to investigate nanocatalysis at single-molecule and single-nanoparticle levels with single-turnover resolution.[9] In this work, by combining SMFM with the traditional electrocatalytic system,[10] we studied the long-term operation stability or deactivation process of a Pt/C electrocatalyst for the HOR by coupling a Pt-catalyzed fluorogenic reaction[11] with the Pt-electrocatalyzed HOR tandemly at single-molecule and single-nanoparticle levels, and revealed a series of new information about the electrocatalytic HOR-induced decay pattern of the catalytic activity of Pt/C. The fluorogenic reaction catalyzed by individual Pt nanoparticles was employed to probe long-term activity variations of individual Pt nanoparticle electrocatalysts during the HOR. The results indicate that the performance decay of Pt/C could be mainly attributed to the electrocatalysis-induced etching of Pt nanoparticles. Spontaneous regeneration of the activity and incubation period of individual Pt electrocatalysts were also observed for the first time. The electro-deactivation kinetics of Pt/C has also been discussed.

For single-molecule nanocatalysis experiments, graphene-supported Pt (Pt/G, with Pt 0.1 wt%) was prepared first with small Pt nanoparticles sparsely dispersed on graphene (Figure 1a; Figure S1 in the Supporting Information); then one end of a microelectrode (a single carbon microfiber; $\varphi \approx 10\,\mu m$) was dipped into an ink prepared with 0.1 mg Pt/G + 50μL Nafion solution (5 wt%) + 950μL ethanol and sonicated for 30 minutes to form many flagellum-like smaller-sized carbon microfibers; the Pt/G catalyst was sparsely dispersed on and electrically contacted with these fibers (scheme shown in Figure 1b). After that, the carbon fiber microelectrode was lay down over a quartz slide surface to be used as working (W) electrode in microflow cell (Figure 1c). A thin strip of Pt foil was used as counter electrode (C); a saturated calomel electrode was used as reference (R). A Pt-catalyzed (in open circuit with no potential applied) fluorogenic reduction reaction of Resazurin by hydrogen (H_2) to Resorufin (**R2** in Figure 1d; more experimental details can be found in the Supporting Information) was used as probe to monitor the Pt-electrocatalyzed HOR-induced (**R1** in Figure 1d) activity decay of individual Pt nanoparticles before and after the long-term electrocatalytic process (**R1**) based on SMFM (Figure 1c).[9d] By detecting the fluorescence signal (excited by a 532 nm green laser) of individual product molecules Resorufin from **R2** one by

[*] Dr. Y. Zhang, T. Chen, Prof. Dr. W. Xu
State Key Laboratory of Electroanalytical Chemistry, Changchun Institute of Applied Chemistry, Chinese Academy of Science
5625 Renmin Street, Changchun 130022 (P.R. China)
and
Jilin Province Key Laboratory of Low Carbon Chemical Power, Changchun Institute of Applied Chemistry, Chinese Academy of Science
5625 Renmin Street, Changchun 130022 (P.R. China)
E-mail: weilinxu@ciac.ac.cn
T. Chen
Graduate University of Chinese Academy of Science
Beijing, 100049 (China)
Dr. S. Alia, Prof. B. S. Pivovar
National Renewable Energy Laboratory
Golden, CO 80401 (USA)

Supporting information for this article is available on the WWW under http://dx.doi.org/10.1002/anie.201511071.

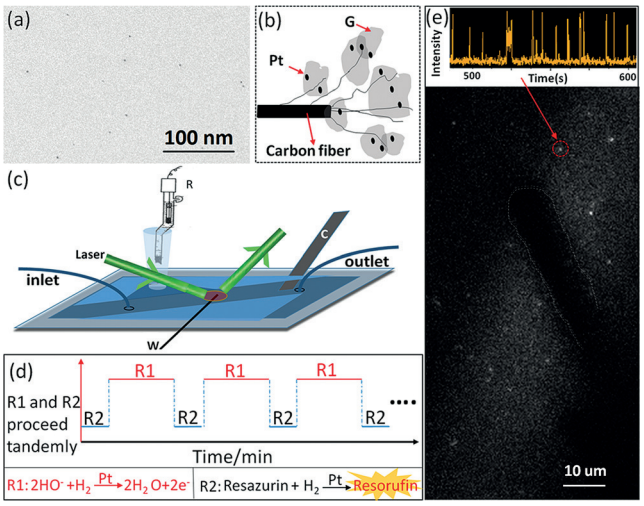

Figure 1. a) Typical TEM image of Pt/G (Pt 0.1 wt %). b) Scheme for the dispersion of Pt/G on carbon fiber microelectrode. c) Combination of microflow cell with electrochemical system; W: working electrode, C: counter electrode, R: reference electrode. d) Scheme for the coupling of Pt-catalyzed **R1** and **R2** tandemly. e) Typical optical image (45×88 um^2) for single-molecule nanocatalysis. The carbon fiber microelectrode was marked with a dotted white line. The top inset shows a typical fluorescence intensity versus time trajectory for **R2** obtained from the location indicated by a red circle on the optical image.

one,[9b] we can monitor the variation of catalytic activity of individual Pt nanoparticle supported on graphene after a long-term electrocatalytic process of the **R1** reaction.

To observe the HOR-induced activity decay of individual Pt nanocatalysts, a tiny area around the end of a microfiber was focused as an observing window. As shown in Figure 1e, with a continuous flow of substrate solution (1 nM Resazurin in H_2-saturated 10 mM phosphate buffer, pH 7.3), the Pt-catalyzed fluorogenic reaction (**R2**) occurs with the formation of fluorescent Resorufin molecules (bright spots) on different locations around the tiny microelectrode (indicated by a dotted line) where the Pt nanoparticles are supported sparsely on a graphene surface which connects electrically with the carbon microelectrode (Figure 1b). The inset in Figure 1e shows part of a typical time trajectory of fluorescence intensity from a location indicated by a red circle in Figure 1e. The bursts on trajectory indicate the formation of fluorescent product molecules on a Pt nanoparticle surface and the dissociation shortly after their formation one by one.[9b] The product formation rate or the burst frequency directly reflects the catalytic activity of individual Pt nanoparticles for **R2**. For Pt-electrocatalyzed **R1**, the three-microelectrode system was connected with a CHI 750 platform for electrochemical measurement. With a continuous flow of substrate solution (10 mM phosphate buffer (pH 7.3) with H_2 saturated), a cyclic voltammetry (CV) scan was performed on the working electrode with Pt/G in the potential range from −0.6 to 0.6 V continuously for four hours (Figures S3, S4).

According to the reaction scheme shown in Figure 1d, the catalytic activity of Pt/G was evaluated by the fluorogenic reaction (**R2**) from a 30-minutes movie before and after each period of CV (**R1**) scan in the same area. First, we monitor the variation of the number of active particles (see the Supporting Information) which are visible through the formation of fluorescent product molecules (**R2**) under SMFM and then counted individually in the same area before/after each period of the CV scan (**R1**). The position of an active particle was determined from a location on which the fluorescent product molecules are formed and dissociate locally one by one (see the Supporting Information). Interestingly, it was found, in a fixed area, initially there are many particles showing catalytic activity for **R2**; as the electrocatalytic **R1** reaction goes on, some individual particles show gradual and irreversible deactivation with fewer and fewer fluorescence signals (Figure S5). Statistically, the total number of active particles (N_{tot}) decreases exponentially with **R1** reaction time (Figure S6). According to the difference of deactivation rates,[12] the active particles could be divided into two types qualitatively (Figure S5e): one is the type of particles which possess higher initial catalytic activity (average turnover frequency per particle, $TOF_{Ave} = 16.3\ min^{-1}$) but deactivate very fast; the other is the type of particles which possess lower initial catalytic activity ($TOF_{Ave} = 11.5\ min^{-1}$) but deactivate slowly. Based on this simple differentiation, the statistic result shown in Figure S6 was deconvoluted into a multiexponential function ([Eq. (1)]),

$$N_{tot} = a \cdot \exp(-b \cdot t) + (N_{tot,0} - a) \cdot \exp(-d \cdot t) \quad (1)$$

where the first term is the contribution from fast decay particles, the second term is from slowly decaying particles; the parameters a and $N_{tot,0}-a$ are the numbers of fast and slowly decaying nanoparticles in the fresh catalyst, respectively; the parameters b and d are the corresponding decay rate constants of the particle numbers (min^{-1}). It was found that $b = 0.018 \pm 0.004\ min^{-1}$ and $d = 0.0016 \pm 0.0010\ min^{-1}$, indicating that the decay number of highly active particles is 12 times faster than that of the less active particles. From the obtained values of a ($= 43 \pm 6$), it can be deduced that the portion of fast decaying particles is about 77 % (x_f), the remainder (23 %) is the portion of slowly decaying particles (x_s).

What is the reason for the deactivation or disappearance of active nanoparticles for **R2**? As for the solution-flow- or **R2**-induced detachment or dissolution of Pt nanoparticles (shown in the TEM images in Figure 2a,b and the Supporting Information) for the same area, after 12 h continuous solution flow (1 nM Resazurin and 10 mM phosphate buffer (pH 7.3) saturated with hydrogen) without any electrochemical reaction, the loss or detachment of Pt nanoparticles from Pt/G (Pt 1 wt %) was less than 5 % and no decrease in size occurred (Figure S7), indicating that the contribution of pure-flow or fluorogenic reaction (**R2**)-induced detachment or dissolution/etching of Pt nanoparticles to the observed fast deactivation or disappearance of Pt nanoparticles (Figure S6) could be neglected. As for the possible chemical poisoning of the fluorogenic reaction (**R2**) to Pt nanoparticles, control experiments show that the long-term (4 h) **R2** reaction only leads to a 20 % decrease of the TOF_{Ave} per particle and 10 %

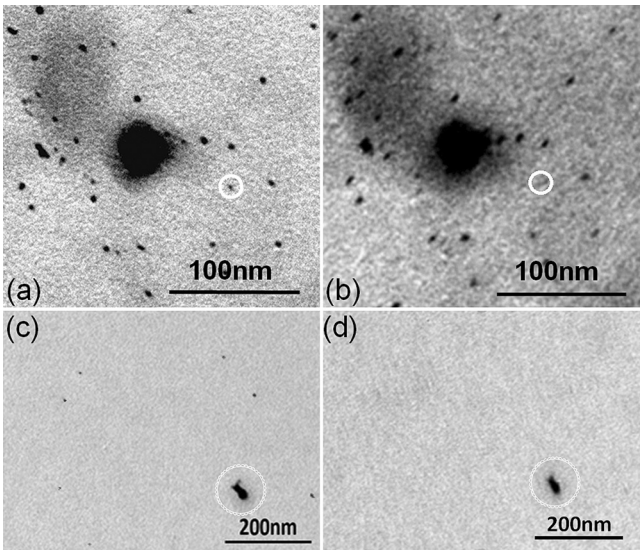

Figure 2. a) TEM image of Pt/G (Pt 1 wt%) dispersed on Au-grid before the solution (1 nM Resazurin and 10 mM phosphate buffer (pH 7.3)with hydrogen saturated) flow. b) TEM image in the same area shown in (a) after the solution flow and water wash of the Au grid. The white circles indicate the loss of a particle. c) TEM image of Pt/G (Pt 1 wt%) before electrocatalytic HOR reaction. d) TEM image after 12 h Pt-electrocatalyzed HOR reaction in the same area shown in (c). The white circles indicate a mark used to find this area after the HOR. All these TEM images were taken on Au-grid-supported carbon film.

deactivation or disappearance of observable active particles and no observable decay of TOF_{Ave} during each **R2** (Supporting Information), all much lower than the corresponding decreases (82% in TOF_{Ave}, 90% in total of the number of active particles, respectively) with electrocatalytic HOR occurring, indicating that the Pt-catalyzed **R2** reaction contributes hardly to the observed fast deactivation or disappearance of the active particles (Figure S6). Also ensemble control experiments indicate that the pure continuous CV in N_2-saturated solution without HOR process would not lead to the HOR performance decay of Pt/G (Figure S8). Then the fast deactivation or disappearance of active particles shown in Figure S6 only can be attributed to HOR (**R1**)-induced either chemical poisoning or electro-etching of Pt nanoparticles, or both.

In order to further verify this point, we did control experiments by transition electron microscopy to check the morphology variance of Pt/G before/after a long-term (12 h) Pt-electrocatalyzed HOR process on the same working area (Figure S9). Interestingly, as an example shows in the TEM images (Figure 2c,d) for Pt/G, statistically, most (>90%) of the small Pt nanoparticles disappeared physically after 12 h of the electrochemical HOR process. The disappearance could not be attributed to the flow-induced detachment because of the fact shown in Figure 2a,b. The physical disappearance of small Pt nanoparticles only can be attributed to the electro-etching or dissolving of Pt nanoparticles induced by the Pt-electrocatalyzed HOR process. The blurred image of a large Pt nanoparticle (indicated by a white dotted circle in Figure 2c,d) after a long-term HOR electrocatalytic process further confirms the HOR-induced electro-etching or dissolution of Pt nanoparticles.[13] Similar the HOR-induced electro-etching phenomena was also observed on individual Pt nanoprism (Figure S10).[14] The electrocorrosion of the carbon support may also contribute in part to platinum loss since the carbon corrosion can result in a fall-off of Pt nanoparticles from the support.[8] These facts indicate that the fast deactivation or disappearance of Pt nanoparticles (Figure S6) observed from **R2** after HOR is indeed mainly because of physical loss or electro-etching of Pt nanoparticles rather than the chemical deactivation induced by strong chemical binding or poisoning of some intermediates to a Pt nanoparticle surface. This conclusion is further confirmed by X-ray photoelectron spectroscopy (XPS) analysis of the sample before/after a long-term HOR process on Pt/G (Figure S11). The fast deactivation or disappearance of particles (Figure S6) after CV scans can then be attributed to the fast electro-etching of Pt nanoparticles. The surface of Pt nanoparticles with higher catalytic activity restructures faster because of the catalysis-induced restructuring, then leading to faster etching of Pt nanoparticles.[4a] The above results also indicate that the surface atoms of Pt nanoparticles are much less stable under an electrocatalytic process (**R1**) than that under heterogeneous catalysis of **R2**, probably because of the strong effect of the electric field.

Furthermore, we studied the deactivation process of slowly decaying particles, defined as the particles which are still alive for **R2** after 4 h of CV of the HOR. The TOF_{Ave} per slowly decaying particle was obtained from each movie after different times of HOR catalytic process. As shown in Figure 3a, the TOF_{Ave} for **R2** shows an exponential decay with the HOR reaction (**R1**) time. By fitting it with a single exponential function: $TOF_{Ave} \propto \exp(-r_s \cdot t)$, the slow decay rate

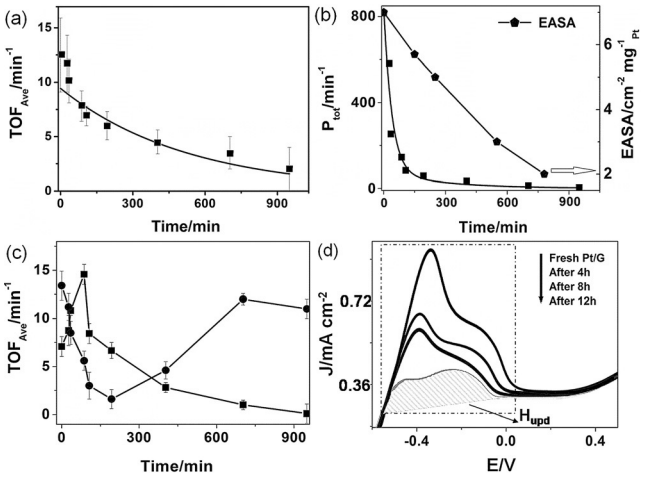

Figure 3. a) The R1 reaction time dependence of the TOF_{Ave} per particle obtained from observable slowly decaying active particles. The solid line is the single-exponential fitting. b) The R1 reaction time dependence (■) of the P_{tot} for all observable active particles and the exponential fitting (black line) based on Equation (2). The curve marked with full pentagons is the R1 reaction time dependence of EASA obtained from H_{upd}. c) ●: spontaneous regeneration of a single Pt nanoparticle; ■: the observation of incubation period on an individual nanocatalyst. d) H_{upd} region in ensemble static linear sweep voltammetry shows the HOR-induced performance decay of Pt/G (Pt 1 wt%) for HOR.

constant (r_s) of TOF_{Ave} per particle was obtained to be about $0.0019 \pm 0.0005\ min^{-1}$. Obviously, the TOF_{Ave} decay observed here could be mainly attributed to the size decrease of individual Pt nanoparticles induced by the electrocatalysis-induced etching shown in Figure 2.[9b]

On the other hand, in order to consider the effects of both decays of TOF_{Ave} per particle and the total number of active particles (N_{tot}) on the total performance (P_{tot}) of the catalyst, the HOR (**R1**)-induced decay process of P_{tot} for **R2** on a whole observing window was studied statistically by combining the decays ($P_{tot} = TOF_{Ave} \cdot N_{tot}$) of both TOF_{Ave} per particle and N_{tot} after each period of CV scans. As shown in Figure 3b, the decay of P_{tot} includes two contributions: one is from fast decaying nanoparticles; the other is from slowly decaying nanoparticles. While each contribution contains two terms, one is the decay number of active particles ($N_{tot,i}$, i = f for fast or s for slow), the other is the decay of $TOF_{Ave,i}$ per particle. Equation (2) reads,

$$P_{tot} = P_f \exp(-b \cdot t) \cdot \exp(-r_f \cdot t) + P_s \exp(-d \cdot t) \cdot \exp(-r_s \cdot t) \qquad (2)$$

where P_f and P_s are the performance contributions of fast decaying nanoparticles and slowly decaying nanoparticles to the total performance of fresh catalyst ($t = 0$), respectively. Based on the already obtained parameters ($b = 0.018 \pm 0.004\ min^{-1}$, $d = 0.0016 \pm 0.0010\ min^{-1}$ and $r_s = 0.0019 \pm 0.0005\ min^{-1}$) from Figure S6 and Figure 3a, the rate constant for fast decay (r_f) of TOF_{Ave} per particle was obtained to be about $0.0075 \pm 0.0048\ min^{-1}$, that is, four times the slow decay rate constant. While the obtained $P_f = 757 \pm 112\ min^{-1}$ and $P_s = 75 \pm 62\ min^{-1}$ indicate that the total performance of fresh catalyst was mainly obtained from fast decaying nanoparticles with high initial activity.

Moreover, we also observed spontaneous activity regeneration after deactivation and incubation period of individual Pt nanocatalysts. As the example shows in Figure 3c for the regeneration (●), this nanoparticle initially shows high catalytic activity with a TOF of $13.4\ min^{-1}$ for reaction **R2**, after a few periods of electrocatalytic HOR reaction (**R1**) through CV scans; the TOF for **R2** decreases hugely to $1.6\ min^{-1}$; while with longer a **R1** process, the TOF for **R2** on this nanoparticle increases inversely to $12\ min^{-1}$ step by step, indicating an effective activity regeneration of the Pt nanoparticle. As for the incubation period observed on individual Pt nanoparticles, as shown in Figure 3c (■), initially, this particle shows very low activity for **R2**, as the electrocatalytic HOR reaction (**R1**) proceeds, the activity for **R2** increases gradually; after a maximum TOF of $14.5\ min^{-1}$, its activity for **R2** decreases inversely, which is a normal deactivation process. Statistically, about 2% of the observable Pt nanoparticles show such kind of activity regeneration, and 3% of the nanoparticles show incubation period. According to previous results,[15] the activity regeneration of nanocatalysts could be mainly attributed to the binding/unbinding of some chemical intermediates on nanoparticle surface. In this case, the poisonous intermediates with strong binding on Pt could be the byproducts from carbon oxidation or corrosion since the long-term **R2** reaction only leads to a negligible effect on the performance of Pt/G for **R1** (Figure S12).[5b,16] As for the incubation period observed here on individual particle, it could be attributed to the gradual exposure or formation of fresh active sites on the particle surface.[12]

As shown above, the catalytic activity of Pt/G for fluorogenic reaction (**R2**) shows a gradual decay during the Pt-electrocatalyzed HOR reaction (**R1**). All the results indicate that the activity decay of Pt/G for **R2** is mainly induced by the Pt-electrocatalyzed HOR process. But it is still not clear whether there is any correlation between the two decays of catalytic activity for **R2** and the electrocatalytic activity for **R1**. Obviously, the single-molecule nanocatalysis experiments alone cannot give us any direct information about the HOR-induced variance of electrocatalytic activity of Pt for HOR. In order to get some clue about the HOR self-induced activity decay of Pt for the HOR, we studied the time-dependent HOR activity of Pt after a certain period of the CV scan in H_2-saturated solution at ensemble level. As shown in Figure 3d, the electrochemically active surface areas (EASAs) of Pt/G were obtained from hydrogen adsorbed/desorbed layers in the so-called H_{upd} region.[17] As shown in Figure 3b, the obtained EASA shows a clear negative correlation with times of CV scans for HOR on Pt/G, unambiguously indicating that the continuous HOR on Pt can lead to a decrease of EASA because of the Pt etching or dissolution, consistent with TEM results (Figure 2c,d and Figure S10), and then a decrease of the total performance of Pt/G for HOR itself. Interestingly, the HOR-induced performance decay for HOR (**R1**) observed above at ensemble level shown in Figure 3b is similar to that observed for HOR-induced decay of P_{tot} for reaction **R2** at single-particle level, confirming that the observed HOR-induced performance decay of Pt for **R2** indeed can be used as a probe to reliably characterize the HOR-induced performance decay of Pt for HOR itself at single-molecule and singe-nanoparticle levels. In principle, such kind of fluorogenic reaction can be used extensively to probe many other kinds of catalytic reaction-induced catalytic activity decay at single-nanoparticle level, such as the ORR-induced activity decay of Pt in fuel cells.

In conclusion, by combining SMFM with traditional the electrochemical method, we studied the HOR-induced real-time deactivation kinetics of the Pt/C electrocatalyst at single-molecule and single-nanoparticle levels. The decay of catalytic performance of Pt/C mainly could be attributed to the electrocatalysis-induced electro-etching of Pt nanoparticles. The less active but highly stable active particles determine the long-term operation stability of nanocatalysts. These new understandings are useful for the rational design of high efficient functional materials.

Acknowledgements

Work was funded by the National Basic Research Program of China (973 Program, grant numbers2012CB932800 and 2014CB932700), National Natural Science Foundation of China (grant numbers 21422307, 21433003, 21573215, 21503212, 21503211, and 21303180), and the Recruitment Program of Global youth Experts of China.

Keywords: deactivation · electrocatalysis · electrochemistry · platinum · single-molecule fluorescence

How to cite: *Angew. Chem. Int. Ed.* **2016**, *55*, 3086–3090
Angew. Chem. **2016**, *128*, 3138–3142

[1] S. J. Hwang, S.-K. Kim, J.-G. Lee, S.-C. Lee, J. H. Jang, P. Kim, T.-H. Lim, Y.-E. Sung, S. J. Yoo, *J. Am. Chem. Soc.* **2012**, *134*, 19508–19511.
[2] M. Moreno, F. J. Ibanez, J. B. Jasinski, F. P. Zamborini, *J. Am. Chem. Soc.* **2011**, *133*, 4389–4397.
[3] a) C. H. Bartholomew, *Appl. Catal. A* **2001**, *212*, 17–60; b) Y. Zhou, S. Wang, K. Zhang, X. Jiang, *Angew. Chem. Int. Ed.* **2008**, *47*, 7454–7456; *Angew. Chem.* **2008**, *120*, 7564–7566.
[4] a) L. Tang, B. Han, K. Persson, C. Friesen, T. He, K. Sieradzki, G. Ceder, *J. Am. Chem. Soc.* **2009**, *132*, 596–600; b) V. Polshettiwar, T. Asefa, *Nanocatalysis: Synthesis and Applications*, Wiley, Hoboken, **2013**.
[5] a) S. Völkening, K. Bedurftig, K. Jacobi, J. Wintterlin, G. Ertl, *Phys. Rev. Lett.* **1999**, *83*, 2672–2675; b) X. W. Yu, S. Y. Ye, *J. Power Sources* **2007**, *172*, 145–154.
[6] S. H. Sun, F. Jaouen, J. P. Dodelet, *Adv. Mater.* **2008**, *20*, 3900–3904.
[7] M. K. Debe, *Nature* **2012**, *486*, 43–51.
[8] D. A. Stevens, M. T. Hicks, G. M. Haugen, J. R. Dahn, *J. Electrochem. Soc.* **2005**, *152*, A2309–A2315.
[9] a) I. L. C. Buurmans, B. M. Weckhuysen, *Nat. Chem.* **2012**, *4*, 873–886; b) W. Xu, J. S. Kong, Y.-T. E. Yeh, P. Chen, *Nat. Mater.* **2008**, *7*, 992–996; c) M. B. J. Roeffaers, B. F. Sels, H. Uji-i, F. C. De Schryver, P. A. Jacobs, D. E. De Vos, J. Hofkens, *Nature* **2006**, *439*, 572–575; d) X. Zhou, W. Xu, G. Liu, D. Panda, P. Chen, *J. Am. Chem. Soc.* **2010**, *132*, 138–146; e) R. Han, J. W. Ha, C. Xiao, Y. Pei, Z. Qi, B. Dong, N. L. Bormann, W. Huang, N. Fang, *Angew. Chem. Int. Ed.* **2014**, *53*, 12865–12869; *Angew. Chem.* **2014**, *126*, 13079–13083; f) T. Tachikawa, S. Yamashita, T. Majima, *J. Am. Chem. Soc.* **2011**, *133*, 7197–7204; g) T. Cordes, S. A. Blum, *Nat. Chem.* **2013**, *5*, 993–999.
[10] J. H. Park, S. N. Thorgaard, B. Zhang, A. J. Bard, *J. Am. Chem. Soc.* **2013**, *135*, 5258–5261.
[11] K. S. Han, G. Liu, X. Zhou, R. E. Medina, P. Chen, *Nano Lett.* **2012**, *12*, 1253–1259.
[12] F. Alhumaidan, D. Cresswell, A. Garforth, *Ind. Eng. Chem. Res.* **2010**, *49*, 9764–9770.
[13] W. Vielstich, in *Handbook of Fuel Cells: Fundamentals, Technology, Applications, Vol. 5–6* (Eds.: H. A. Gasteiger, H. Yokokawa), Wiley, Hoboken, **2009**.
[14] B. A. Larsen, K. C. Neyerlin, J. B. Bult, C. Bochert, J. L. Blackburn, S. S. Kocha, B. S. Pivovar, *J. Electrochem. Soc.* **2012**, *159*, F622–F627.
[15] Y. Lei, H. Y. Zhao, R. D. Rivas, S. Lee, B. Liu, J. L. Lu, E. Stach, R. E. Winans, K. W. Chapman, J. P. Greeley, J. T. Miller, P. J. Chupas, J. W. Elam, *J. Am. Chem. Soc.* **2014**, *136*, 9320–9326.
[16] I. Kvande, D. Chen, T.-J. Zhao, I. M. Skoe, J. C. Walmsley, M. Rønning, *Top. Catal.* **2009**, *52*, 664–674.
[17] Y. Ishikawa, J. J. Mateo, D. A. Tryk, C. R. Cabrera, *J. Electroanal. Chem.* **2007**, *607*, 37–46.

Received: November 28, 2015
Published online: January 28, 2016

